Materials Chemistry and Physics 143 (2013) 124–132

Contents lists available at ScienceDirect

Materials Chemistry and Physics

journal homepage: www.elsevier.com/locate/matchemphys

Solvent and stabilizer free growth of Ag and Pd nanoparticles using metallic salts/cyclotriphosphazenes mixtures

C. Díaz Valenzuela [a], M.L. Valenzuela [b, *], S. Caceres [a], R. Diaz [a], C. O'Dwyer [c, d]

[a] Departamento de Química, Facultad de Química, Universidad de Chile, La Palmeras 3425, Nuñoa, Casilla 653, Santiago de Chile, Chile
[b] Universidad Andres Bello, Departamento de Ciencias Química, Facultad de Ciencias Exactas, Av. Republica 275, Santiago, Chile
[c] Applied Nanoscience Group, Department of Chemistry, University College Cork, Cork, Ireland
[d] Micro & Nanoelectronics Centre, Tyndall National Institute, Lee Maltings, Cork, Ireland

HIGHLIGHTS

- Pyrolysis $MLn/N_3P_3(O_2C_{12}H_8)_3$ mixtures under air, give Pd and Ag nanoparticles.
- $AgPPh_3[CF_3SO_3]$ and $PdCl_2$ in molar ratios 1:1 and 1:5 were used.
- Metal foams were obtained from 1:5 ratios when deposited on SiO_2.
- Using crucible supporting in 1:1 metal/trimer <2 nm Pd nanoparticles were obtained.
- The probable mechanism involves a dewetting, nucleation and ripening crystallization.

GRAPHICAL ABSTRACT

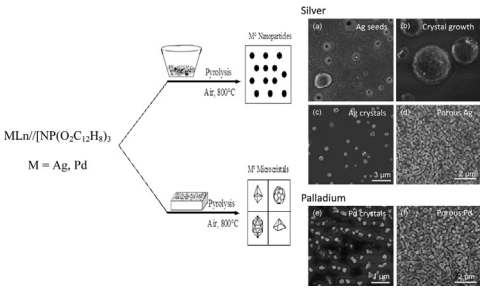

ARTICLE INFO

Article history:
Received 13 March 2013
Received in revised form
29 July 2013
Accepted 23 August 2013

Keywords:
A. Metals
B. Annealing
C. Electron microscopy
D. Surface properties

ABSTRACT

Cyclotriphosphazene is used as a sacrificial solid-state template to synthesize a range of Ag and Pd nanoparticles with diverse geometries by thermal treatment using $MLn/N_3P_3(O_2C_{12}H_8)_3$ mixtures. The Pd and Ag nanoparticles are synthesized by solid-state pyrolysis of $AgPPh_3[CF_3SO_3]/N_3P_3(O_2C_{12}H_8)_3$ and $PdCl_2/N_3P_3(O_2C_{12}H_8)_3$ mixtures with molar relationships of 1:1, 1:5 and 1:10 respectively, in air and at 800 °C. The morphology of the as-prepared nanoparticles is found to depend on the molar ratio of the precursor mixture, the preparation method and of the nature of the metal. Ag and Pd, microcrystals were thermally grown on Si from the respective 1:1 precursors while that metal foams were grown from 1:5 ratios precursors on SiO_2 wafers. High resolution transmission electron microscopy investigations reveal in most cases small crystals of Pd. HRSTEM measurements indicate that the formation of the Pd and Ag nanoparticles occurs through a phase demixing and dewetting mechanism. This approach has potential to be a useful and facile method to prepare metallic nanoparticles without requiring solutions or surfactants for application in electronic, catalytic and sensor materials and devices.

1. Introduction

Although metallic nanoparticles have been extensively studied [1–5], both preparation and mechanism in solution phase, few solid-state synthetic methods have appeared [6]. Most scarce is the solid-state mechanism of formation of nanoparticles. Specifically nanoparticles of Pd have been widely studied and several solution methods have been reported and their catalysts properties extensively studied [7–19]. Since the pioneering work of Turkevich [7] in the preparation, characterization and demonstration of catalytic properties of Pd nanoparticles, several preparative reports have

* Corresponding author.
E-mail address: mlvalenzuela@unab.cl (M.L. Valenzuela).

0254-0584/$ – see front matter © 2013 Elsevier B.V. All rights reserved.
http://dx.doi.org/10.1016/j.matchemphys.2013.08.034

appeared [8–19]. The majority of reports focus on interesting catalytic properties [8,9] but much of the early work neglected the detailed characterization of the Pd nanoparticles, which has been widespread for solution synthesized nanoparticles and nanocrystals. Recently, the growth pathways of Pd nanocrystals in solution have been examined using HRETM in-situ by trapping precursors solutions between sheets of graphene [20]. The most widely used solution based method is that reported by Miyake using H_2PdCl_4 or M_2PdCl_4 (M = Na or K salt as the source of metal), with poly(*N*-vinylpyrrolidone) (PVP) acting as stabilizer in an alcoholic solvent [10]. In such synthetic protocols, the type of alcohol and its water content strongly influence the resulting size of the nanoparticles.

A variant of the original Brust–Schiffrin approach using H_2PdCl_4 as precursor has been also reported [11]. Additionally, a modified Turkevich [12] method has also been adapted so that rectangular Pd nanoparticles could be obtained, which uses K_2PdCl_4, ascorbic acid and CTAB as surfactant. Electrochemical methods have also become attractive options for Pd and other nanocrystal growth [13]. Using a method developed by Chaudret et al. [14] which makes use of organometallic $[Pd(\eta\text{-}C_3H_5)_2Cl]_2$ and $Pd_2(dba)_3$ precursors, nanoparticles of ~2 nm in size can be obtained.

In essence, there are many solution based methods for metallic nanoparticle syntheses and the optimum choice depends not only on the type, shape, size distribution and crystallinity of the resulting crystals, but on their application. Miscellaneous variants such as sonochemical [15], and microwave irradiation [16] approaches can also be used with PVP as stabilizers [17], and the use of highly controlled Au nanoparticles seeds can be used for growing Pd and Ag nanoparticles, and have allowed shape control growth of controlled bimetallic crystal systems [21–23]. More recently micrometric Pd crystals have been prepared from $NaPdCl_4$ using PVP as a stabilizer, allowing a multitude of shapes in the resulting Pd crystals. By varying the reaction time, different morphologies such as single crystals, nanoboxes and nanocages were obtained [19]. The only reported solid state approach for preparing Pd nanoparticles known is through the thermolysis of the $[Pd(S_{12}C_{12}H_{22})_2]_6$ cluster at 325 °C which results in Pd/PdO nanoparticles with a broad distribution of polygonal particles with sizes varying from 20 to 200 nm [24]. Pd nanoparticles deposited on graphite surfaces have also been obtained by pyrolysis of molecular containing Pd clusters in presence of H_2 [25].

Silver (Ag) nanoparticles have also been widely studied and in solution many different and novel 2- and 3-dimensional shapes are possible [26] which have shown an interesting range of plasmonic properties [27–30]. For Ag, there remains a scarcity in solid-state methods for preparing nanoparticles and nanocrystals and their formation mechanism is practically unknown. To the authors' knowledge, two reports exist concerning true solid state formation of Ag nanoparticles: the pyrolysis of the salt $Ag_2(OOC{\equiv}CCOO)$ can result in Ag nanoparticles with sizes in the range 20–30 nm [31] and plasma-enhanced deposition of the silver complex Ag(fod)(PEt_3), (fod = 2,2-dimethyl-6,6,7,7,8,8,8,-heptafluorooctane-3,5-dionato) [32] allows the formation of thin films of ~17 nm. Strategies to control shape and size are not automatically possible using these approaches.

The importance of solid state methods for metallic nanoparticle growth is the need in some instances to have methods that are 'dry' and thus compatible with certain processing requirements, such as interconnects, electrical contacts, SERS sensors for biological species and to prevent a multi-step method that required further understanding of competitive solution interactions which make drop and pin-casting of NP-containing liquids quite difficult to control [33–36]. Some technological applications such as catalysis, water purification and energy storage often require operation of devices at high temperatures (fuel cells) and in the complete absence of liquids or water (Li-based batteries).

Metal foams also called "metallic sponge" and "macroporous metals" [37–45] have attracted the attention due to their unusual and peculiar properties such as mechanical strength and stiffness [37]. These materials can be prepared by several solution methods such as dealloying of M/M′ alloys and by forming a metal-organic composite and eliminating the organic part both through dissolution and/or by calcination. However no solid-state approximations have yet been reported. The here reported method could be a useful and general solid-state route to these type of materials.

We have previously reported [46–57] a new solid state method to prepare M, M_xO_y and $M_xP_yO_z$ nanoparticles using organometallic derivatives of poly and cyclotriphosphazenes as molecular precursors, summarized in Fig. 1. When the respective precursor is unstable or is prepared in low yield, $MLn/N_3P_3[O_2C_{12}H_8]_n$ mixtures can be made as useful precursors of metallic nanostructured materials [58,59] Surprisingly, although the polymer or trimer phosphazene have a chain (in the case of Au [59]) or ring containing phosphorus atoms, the products do not contain metallic phosphates species (except when the metallic precursor compound itself contain phosphorus). Additionally, structures can be formed within porous carbon hosts directly, negating the need for second step dispersal of NPs, both as powders and directly on surfaces. In this work, we report the preparation of Ag and Pd nanoparticles from $AgPPh_3[CF_3SO_3]/[NP(O_2C_{12}H_8)]_3$ and $PdCl_2/[NP(O_2C_{12}H_8)]_3$ precursors. We show that the solid state method can indeed produce phase pure Ag and Pd nanoparticles with non-spherical shapes without ligand assisted growth pathways. Furthermore, since the precursors are mixtures of metallic salts and trimer, phase demixing occurs resulting in a specific dewetting and physics and chemical decomposition mechanisms that greatly influence the growth mechanism and the resulting shape and size distribution.

2. Experimental

2.1. Materials

Palladium chloride (Sigma–Aldrich) was used as purchased. The complex $AgPPh_3[CF_3SO_3]$ was prepared using a reported procedure [60]. The cyclic trimer $[NP(O_2C_{12}H_8)]_3$ was prepared according reported procedures [61].

2.2. Mixture preparation

2.2.1. $PdCl_2/[NP(O_2C_{12}H_8)]_3$ mixture

The respective molar mixture of Palladium chloride (0.1 g, 0.56 mmol for the 1.1 ratio mixture) and (0.14 g, 0.789 mmol for the 1:5 ratio mixture) and the trimer $[NP(O_2C_{12}H_8)]_3$ (0.4 g, 0.58 mmol for the 1.1 ratio mixture and 1.94 g, 2.82 mmol for the 1:5 ratio mixture) were dissolved in CH_2Cl_2, stirred for 24 h and evaporated to dryness in a *vacuum* at room temperature.

2.2.2. $AgPPh_3[CF_3SO_3]/[NP(O_2C_{12}H_8)]_3$ mixture

$AgPPh_3[CF_3SO_3]$ (0.3795 g, 9.583×10^{-4} mmol) and $[NP(O_2C_{12}H_8)]_3$ (0.5130 g, 7.467×10^{-4} mmol) for a molar relationship 1:1; $AgPPh_3[CF_3SO_3]$ (0.074 g, 1.868×10^{-4} mmol) and $[NP(O_2C_{12}H_8)]_3$ (0.4234 g, 6.16×10^{-4} mmol) for a molar relationship 1:5 and $AgPPh_3[CF_3SO_3]$ (0.0594 g, 1.5×10^{-4} mmol) and $[NP(O_2C_{12}H_8)]_3$ (0.4064 g, 5.91×10^{-4} mmol) for a molar relationship 1:10, were stirred in a CH_2Cl_2 solution at room temperature for 24 h. After this the solvent was eliminated under reduced pressure and the solid dried in a *vacuum* at room temperature.

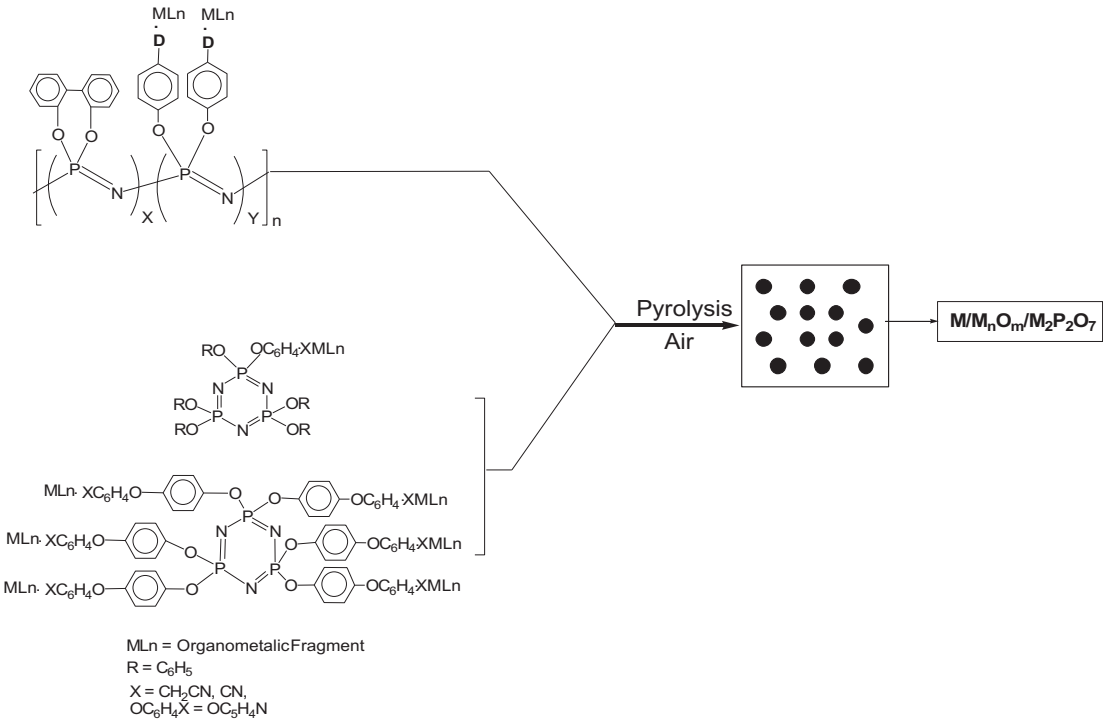

Fig. 1. Schematic representation of the solid-state method for nanostructured material formation using oligomeric and polymeric precursors.

2.3. Characterization methods

Infra-red (IR) spectra were recorded on an FT-IR Perkin–Elmer Spectrum BX II spectrophotometer. X-ray diffraction (XRD) was carried out at room temperature on a Siemens D-5000 diffractometer with $\theta-2\theta$ geometry. The XRD data was collected using Cu-Kα radiation (40 kV and 30 mA). Scanning electron microscopy (SEM) and energy dispersive X-ray analysis (EDX) were acquired with a JEOL 5410 SEM with a NORAN Instrument micro-probe transmission microscope and with a Scanning electron microscopy Hitachi SU-70 FESEM operating at 10 kV equipped with an Oxford Instruments X-max 50 mm^2 solid-state EDX detector. TEM

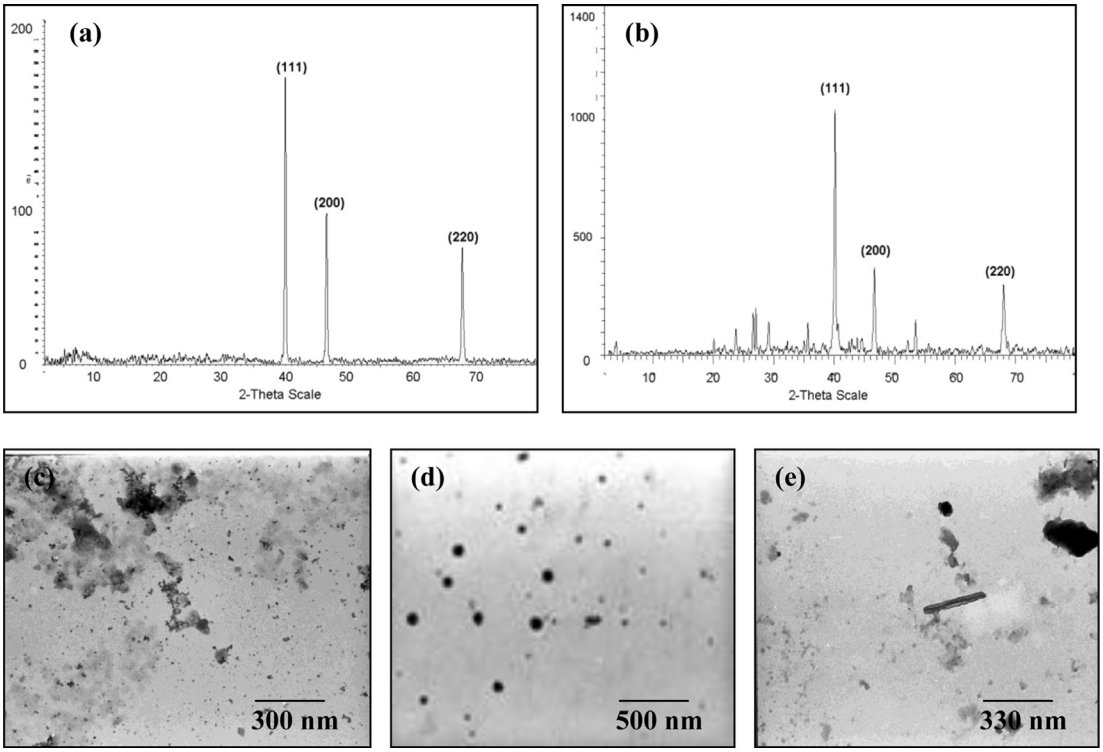

Fig. 2. XRD of the pyrolytic products from the (a) 1:1 mixture, (b) 1:5 mixture, $PdCl_2/[NP(O_2C_{12}H_8)]_3$ and TEM images from the mixtures $PdCl_2/[NP(O_2C_{12}H_8)]_3$ with ratios (c) 1:1, (d) 1:5 and (e) 1:10.

images were recorded on a JEOL SX 100 transmission microscope, using fine powdered samples dispersed in water and dropped on a conventional carbon-wasted copper grid and with a Transmission electron microscopy JEOL JEM-2100F operating at 200 kV. TEM image measurements were made using DigitalMicrograph™ software with a Gatan Multiscan 794 CCD Camera.

2.4. Pyrolysis

The pyrolysis experiments were carried out, as previously reported [46–59], by pouring a weighed portion (0.05–0.15 g) of the gel on aluminum oxide boats placed in a box furnace, heated from 25 to 300 °C and then to 800 °C, and annealed for 2 h.

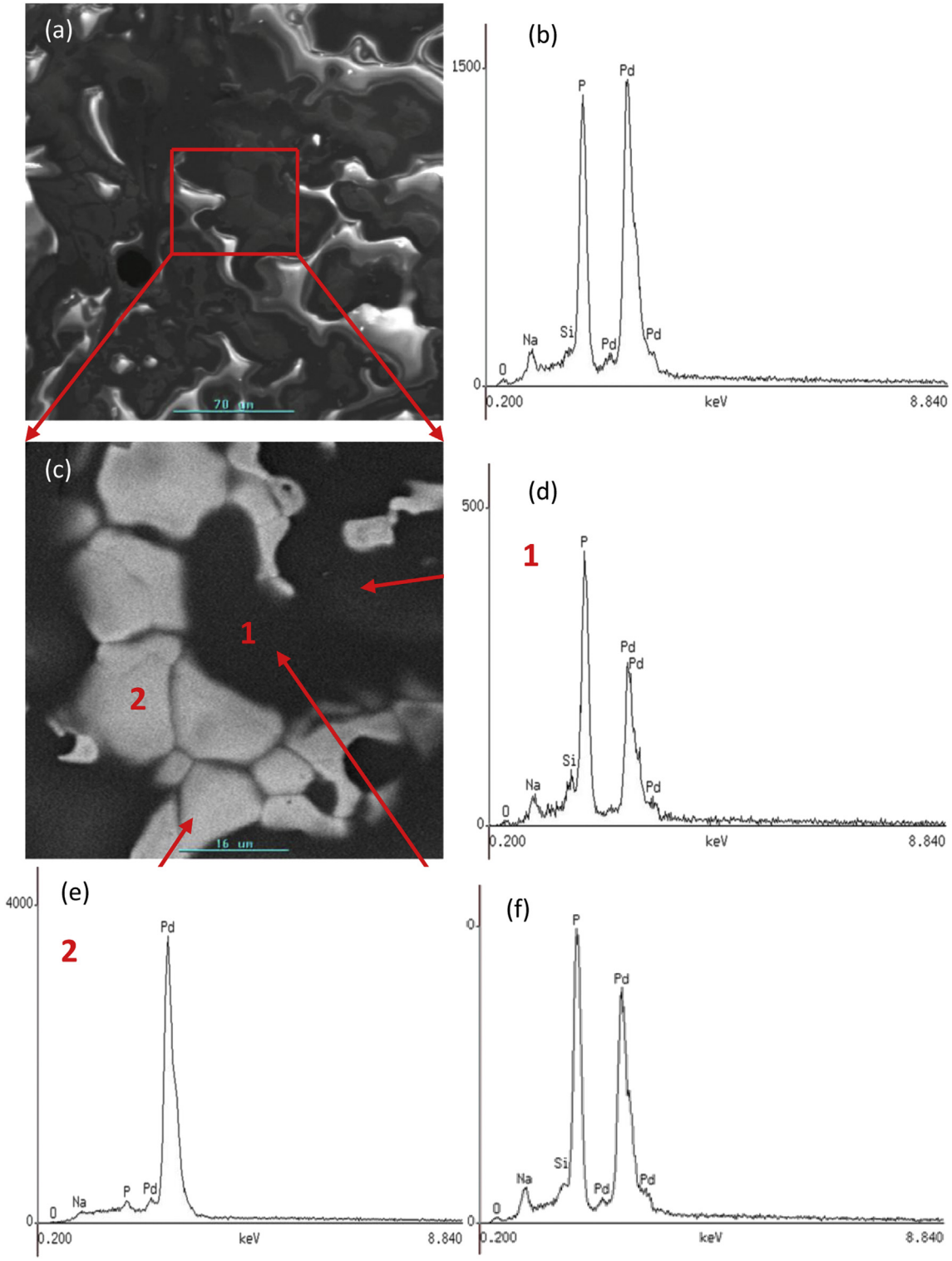

Fig. 3. (a) SEM image of the pyrolytic product from the 1:1 $PdCl_2/[NP(O_2C_{12}H_8)]_3$ mixture and (b) a general EDS analysis. (c) Backscattered SEM image of an increased area detail of the marked zone in (a). EDS in (d) and (f) of P-rich and Pd and regions marked 1 and 2 respectively.

3. Results and discussion

3.1. $PdCl_2/[NP(O_2C_{12}H_8)]_3$ mixture

Pyrolysis of a $PdCl_2/[NP(O_2C_{12}H_8)]_3$ mixture system in air at 800 °C results in single crystal Pd material as evidenced by the XRD patterns shown in Fig. 2a for the pyrolytic products from the 1:1. All XRD patterns of the investigated samples exhibit characteristic (111), (200), (220) planes of Pd from a fcc lattice [10]. The intensity ratios between the (111) and (200) diffraction peaks $I_{(200)}/I_{(111)}$ of the pyrolytic product from these mixtures, are 0.439 which compare well with the standard value 0.458 (PDF 01-088-233). XRD analysis of the 1:5 mixture, see Fig. 2b confirms a ratio for single crystal reflections of 0.457.

Analysis of the resulting nanoparticles confirms that the size distribution depends on the ratio of the $PdCl_2/[NP(O_2C_{12}H_8)]_3$ mixture. As is shown in Fig. 2c–e, the particle size is found to decrease as the metal/polymer relationship increases. From the respective particle size histogram, a mean size of 12 nm and 150 nm were determined for the 1:1 and 1:5 mixture ratios respectively. For the 1:10 $PdCl_2/[NP(O_2C_{12}H_8)]_3$ mixture irregular shapes and/or agglomerates are often found and typically greater than 150 nm in size. However, as is characteristic of this solid state fabrication [6] some zones of agglomerates comprising micrometer sized, granular features are also observed.

Interesting features were also observed by SEM in Fig. 3. Fig. 3a shows a general SEM image and Fig. 3b shows a general EDS analysis. EDS performed on three different zones of this sample in Fig. 3b, d, e, f confirms the formation of zones containing pure granular Pd, Fig. 3e and interspersed within regions of residues containing phosphorus arising from the cyclic phosphazene Fig. 3d, f. Site specific EDS in Fig. 3d confirms the dominant P concentration in the non-metallic residual material. Other pyrolytic products arising from the 1:5 and 1:10 $PdCl_2/[NP(O_2C_{12}H_8)]_3$ mixtures result in a material with a dominant Pd and P content; the consistent P quantity in these mixtures stems from the high molecular weight macromolecular cyclic $NP(O_2C_{12}H_8)]_3$ (see Supplementary material S1).

Morphologies and size nanoparticles depend on the conditions of the pyrolysis of the mixtures *i.e.* we notice an influence on particle size if the pyrolysis was performed on a crucible or on Si and SiO_2 wafers [55]. In this latter method, microcrystals with diverse morphologies diverse were grown as is shown in Fig. 4. The morphologies of the crystals depends both on the molar ratio of the

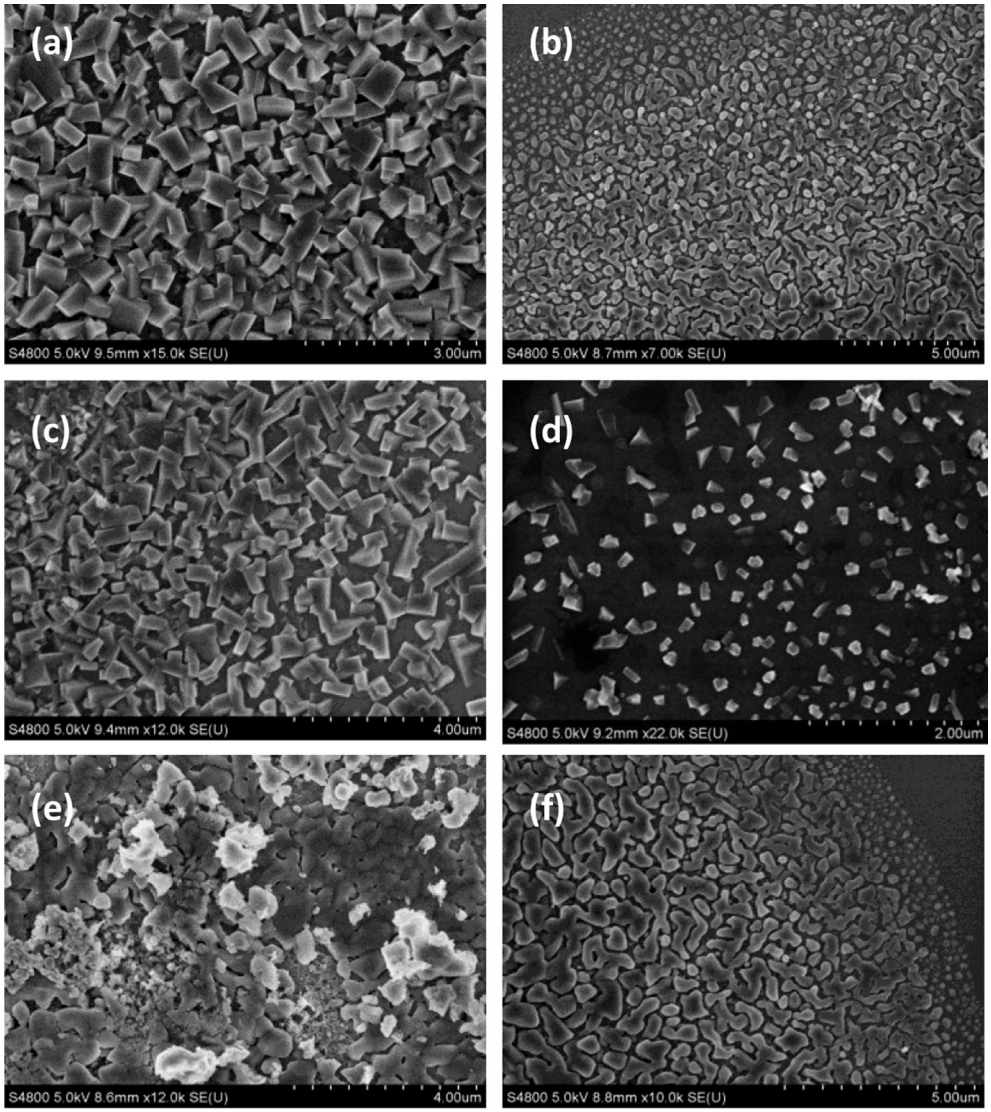

Fig. 4. SEM images of the pyrolytic product from $PdCl_2/[NP(O_2C_{12}H_8)]_3$ (a) 1:1 on Si, (b) 1:5 on SiO_2, (c) 1:5 on Si, (d) 1:5 on SiO_2, (e) 1:1 on Si and (f) 1:1 on SiO_2.

$PdCl_2/[NP(O_2C_{12}H_8)]_3$ mixture and on the Si or SiO_2 substrate. Specifically, the mechanism of the macromolecular precursor deposition under heating is similar, with cleavage of metal centers and their subsequent agglomeration to single crystal nanoparticles. Demixing of the metal- and non-metal-containing phases within the mixture allows spatial patterning due to nucleation dewetting processes. In all cases for all metals thus far studied, carbonization and graphitization of the resulting carbon residue prevent full dewetting of the layer which gives a high density of crystals on the surface.

For the 1:1 precursor deposited on Si, cubic geometries were observed as is shown in Fig. 4a. On the other hand, metallic "foams" are obtained from the 1:5 precursor deposited on SiO_2 as is shown in Fig. 4b. The effect on the substrate deposition is different for the 1:1 or 1:5 mixture ratios. For the 1:5 ratio, similar morphologies are observed but characteristically different to the that found for the same deposit placed on SiO_2,or Si, as can be seen by comparison of Fig. 4c and d respectively. In this case, the influence of a larger mixture fraction of the polymeric component allows thermally driven instability formation within the polymer to dominate, and we thus observe a spinodal-like pattern in the polymer with a dominant wavelength, and ripened crystals located on this pattern.

For the 1:1 ratio a less defined morphology for the resulting crystals was observed on the Si than is found after pyrolysis of the same precursor on SiO_2 (Fig. 4e, f). It appears to be that the different morphologies in similar conditions ie ratio and substrate deposition are different steps of the dewetting mechanism [62–65]. In fact SEM images shown in Supplementary materials S2 confirm the salient features of phase demixing and dewetting involved in the formation of Pd nanoparticles and porous Pd metal foams.

HRTEM images were acquired from materials scraped from the surface grown deposits. A HRTEM image of two single particles, showed in Fig. 5a revealed atomic lattice fringe spacing corresponding to (111) and (200) spacing of cubic (fcc) Pd. The corresponding electron diffraction pattern in Fig. 5b, shows the diffraction rings corresponding to the main lattices facets of fcc Pd and demonstrating the crystalline nature of the nanoparticle. Another two Pd nanoparticles showing two the (111) and (311) diffraction ring of cubic Pd are showed in Fig. 5c and inset. A histogram (see Supplementary materials S3) of ~800 individual particles reveals an average size of 1.8 nm. An EDS analysis of these samples in a region of 50 × 50 nm (see Supplementary materials S4) reveals the presence of only Pd.

3.2. $AgPPh_3[CF_3SO_3]/[NP(O_2C_{12}H_8)]_3$ system

Pyrolysis of a mixture of $AgPPh_3[CF_3SO_3]/[NP(O_2C_{12}H_8)]_3$ in air and at 800 °C, contrary to the Pd precursor, results in a mixture of

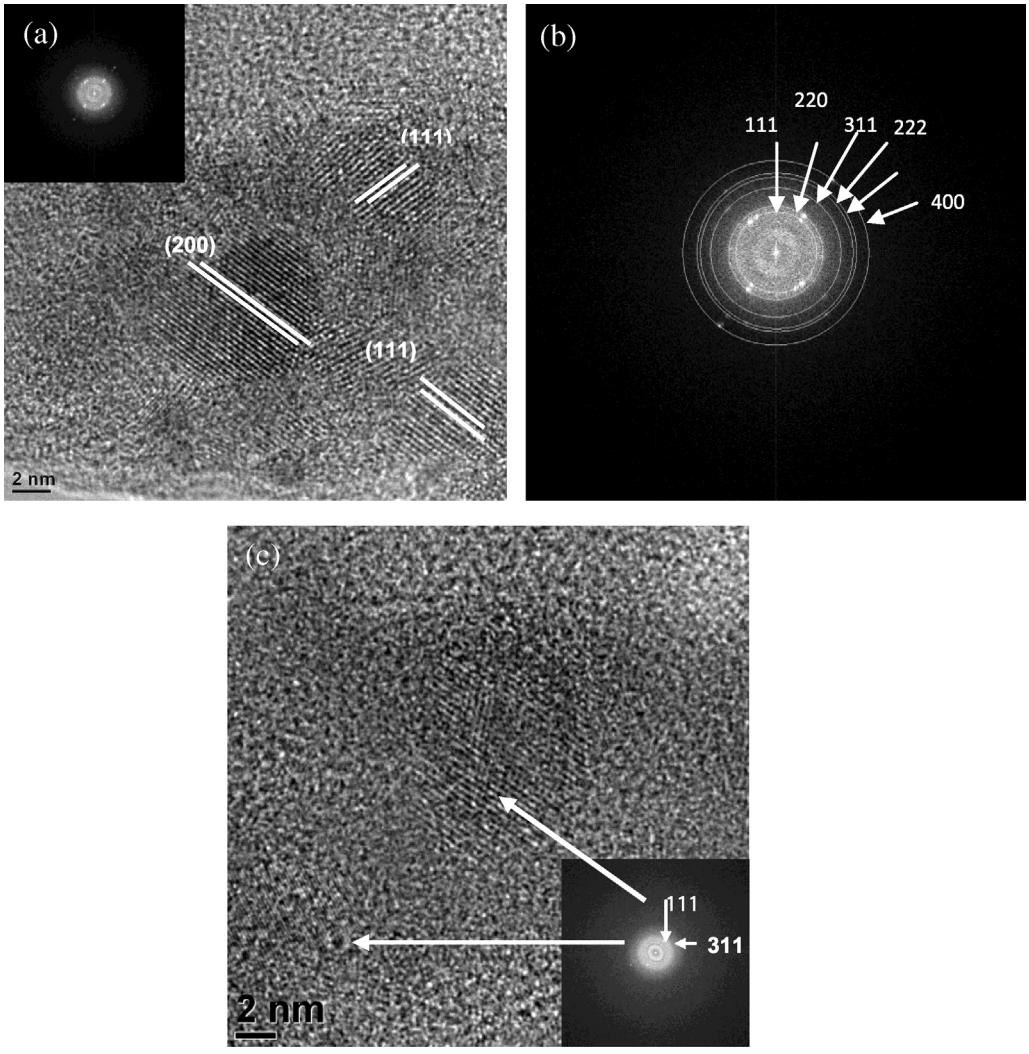

Fig. 5. (a) HRTEM image of two isolated small nanoparticles, (b) their FFT image and (c) another two nanoparticles with their FFT in the inset.

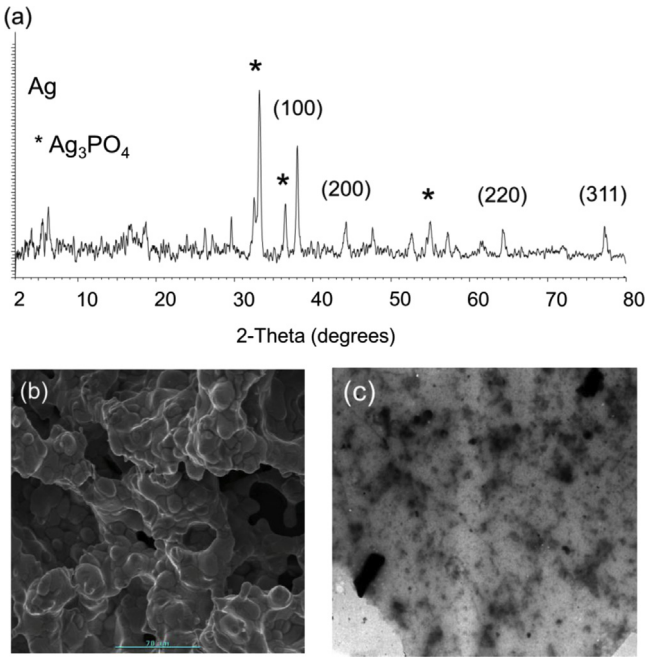

Fig. 6. XRD pattern (a), SEM image (b) and TEM image for the pyrolytic product from the 1:1, $AgPPh_3[CF_3SO_3]/[NP(O_2C_{12}H_8)]_3$ mixture.

nanoparticle phases composed of Ag, Ag_3PO_4 and phosphorus oxides as evidenced by their XRD patterns shown in Fig. 6a. All the XRD patterns of the investigated samples presents the (100), (200), (220) and (311) planes of a fcc lattice of cubic Ag [47]. Also the (210), (211), (310) and (222), (322) and (321) typical of cubic Ag_3PO_4 is clearly observed indicating some crystalline component for this phase [47]. Other less intense peaks around $2\theta = 26–28^\circ$ were assigned to the oxide $(P_4O_6)O_2$. Thus the formation of Ag_3PO_4 together with Ag is typical of the solid-state pyrolysis of Ag containing precursors containing phosphorus atoms both in the polymeric or trimer phosphazene or as ligand of the metal compound [47]. As observed in this another report [47], a silver island over voids of Ag_3PO_4 could to explain the observed XRD patters.

The presence of silver phosphates could be avoided by using a solid-state template that do not containing phosphorus as the PPh_3 ligand. However, the nature of the phosphazenic molecules allows a specific chemical decomposition and also an important physical decomposition which affects the dewetting-mediated formation of nanoparticles and the ripening suprecrystallization of larger faceted crystals. The method also allows the opportunity for pyrophosphates and oxides when transition metals are used rather than noble metals [66]. In fact pyrolysis of mixtures $AgNO_3]/[NP(O_2C_{12}H_8)]_3$ results in only phase pure Ag (see Supplementary materials S5).

The SEM image of the pyrolytic product from the 1:1 $AgPPh_3[CF_3SO_3]/[NP(O_2C_{12}H_8)]_3$ exhibits the typical dense fused-grain morphology of cubic Ag with Ag_3PO_4 formation acting as bridge [47], see Fig. 6b. The TEM images exhibit some irregular forms including larger agglomerates together with some zones with circular isolated Ag nanoparticles see Fig. 6c.

Furthermore, when the pyrolysis is performed on a Si and SiO_2 wafers, microcrystals with different morphologies are grown depending on the relationship of the mixture $AgPPh_3[CF_3SO_3]/N_3P_3(O_2C_{12}H_8)_3$ and on the Si and SiO_2 deposition substrates. For instance, as shown in Fig. 7a, the 1:5 mixture deposited on Si results in imperfect crystals with a large variation in morphology and size. In contrast for the same 1:5 mixture but deposited on SiO_2 substrate, metallic Ag “foams”, which is essentially a 3D porous Ag

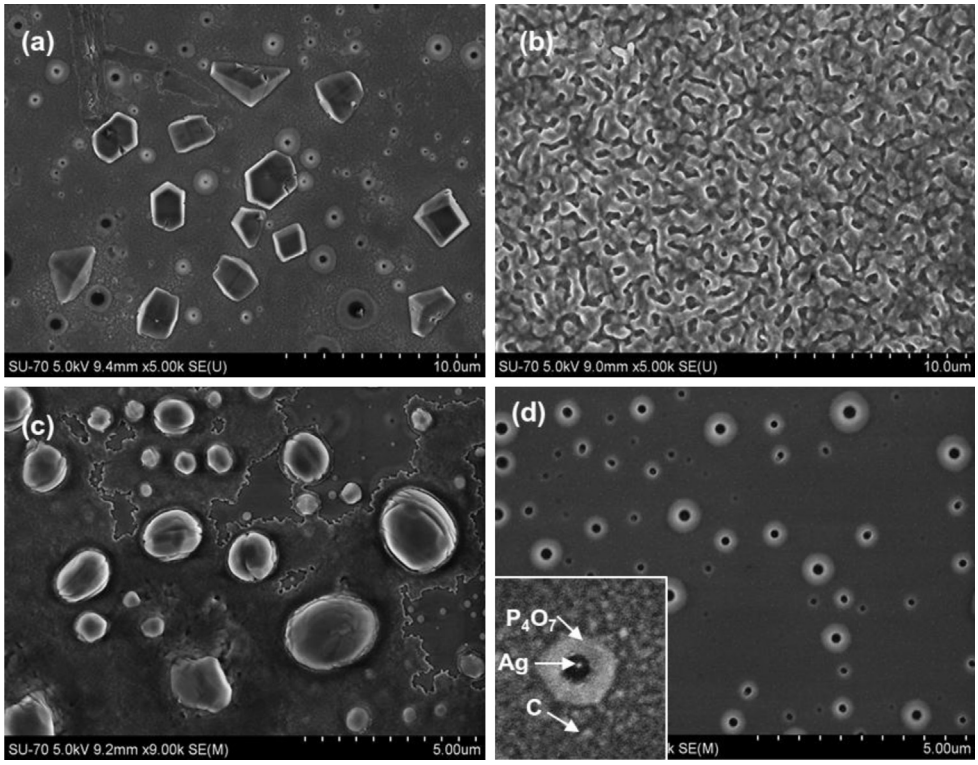

Fig. 7. SEM images of the $AgPPh_3[CF_3SO_3]/[NP(O_2C_{12}H_8)]_3$ mixtures in a molar ratio of (a) 1:5 deposited on Si, (b) 1:5 deposited on SiO_2 where solid state porous Ag is formed, (c) 1:1 deposited on Si in one zone, and (d) 1:1 deposited on Si in another zone prior to the nucleation coarsening and ripening of NPs within the pinholes. (*Inset*) The detail of a pinhole and a spinodally decomposed and solidified carbon support. NPs are located around the rim and the seed of the growing Ag crystal can found inside the pinhole itself.

metal without requiring solution based dealloying, is observed in Fig. 7b. On the other hand for the 1:5 $AgPPh_3[CF_3SO_3]$/$[NP(O_2C_{12}H_8)]_3$ mixture deposited on Si two different morphologies are typically observed in two different zones: dumbbell-like crystals, see Fig. 6c, which are characteristic of Ag when formed also from solution on the nanoscale [67,68] and core/shell structures, as shown in Fig. 6d. These core–shell structures are in fact the pinholes formed during nucleation dewetting of the polymeric mixture, which is halted due to solidification of the carbonized organic matter. NPs form within this matrix and are localized around the rims of these pinholes and the crystal then ripen through nucleation coarsening of these NPs; these pinholes act as incubation sites for crystal growth. For Ag, the phosphate is also formed in the vicinity. SEM analysis of typical patterns and features of this dewetting mediated phase demixing process during pyrolysis and solid state growth, shown in Supplementary materials S6, are reminiscent of a dewetting and decomposition mechanism that involves elements of spinodal decomposition and also Maragoni-type instabilities due to lateral viscosity variations of the metallic nanoparticle-containing mixture during heating, phase separation and crystallization [62–65], that can result in the crystal growth but also their patterning on surfaces.

3.3. Probable mechanism formation

The most likely mechanism for the formation of the Pd and Ag nanostructures may be similar to mechanisms that have been previously established as general for the solid-state pyrolysis of metallic and organometallic derivatives cyclic-oligomer-phosphazene and polyphosphazenes [46–57] and for the metallic salts/cyclotriphosphazene mixtures systems [58,59].

The first step involves the cross-linking [46] of the cyclotriphosphazene units as shown in Fig. 8, induced by the coordination of the metal centers, during the initial annealing step. The subsequent carbonization of the organic matter produces holes or voids were the metal centers begin to coarsen and grow. Carbonization of the organic matter usually occurs during pyrolysis of metallic and organometallic derivatives of polymers around 350 °C [57]. Some incomplete combustion always produces some CO [38] which reduces the metallic Pd(II) and Ag(I) salts to Pd° and Ag° which coarsen at high temperature. Also in the combustion process, often a sudden loss of nitrogen – arises from the PN groups of cyclotriphosphazene – which can induce foamy materials through rapid expulsion of the gas during solidification [37–45].

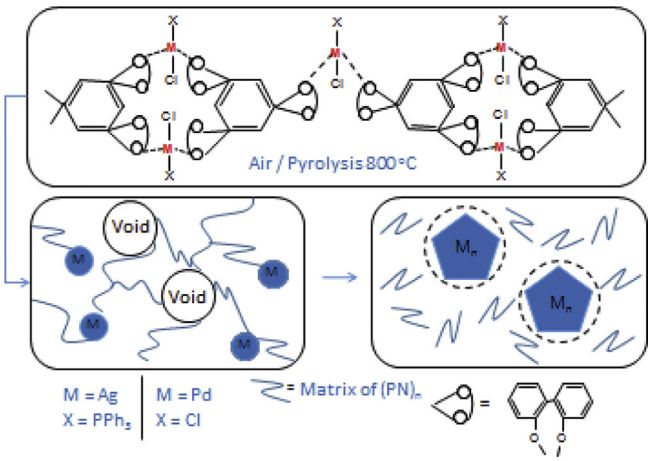

Fig. 8. Schematic representation of the probable formation mechanism of the Pd and Ag nanostructured materials.

4. Conclusion

In summary, we have explored a new and facile solid-state approach to prepare Pd and Ag metallic nanoparticles using the mixtures of $AgPPh_3[CF_3SO_3]$/$[NP(O_2C_{12}H_8)]_3$ and $PdCl_2$/$[NP(O_2C_{12}H_8)_3$. The morphology and the particle size are found to be very sensitive to the preparation and deposition methods used.

By tuning the metal/trimer and the substrate on deposit the mixtures a possible way to control the morphologies and size of products in solid state is proposed using chemical and physical decomposition and dewetting mechanism, including nucleation and ripening crystallization of NPs. Using the 1:5 mixtures on SiO_2, metal foams are grown for both metal, while a 1:5 ratio mixture deposited on Si results in well-defined Ag and Pd crystals. As recently observed for the Au/trimer mixtures [59], and using the crucible as supporting for the pyrolysis in the 1:1 metal/trimer relationships, very small (<2 nm) Pd nanoparticles were obtained. The method allow the possibility to tune the structure of metal foams by using 1:5 mixtures $AgPPh_3[CF_3SO_3]$/$[NP(O_2C_{12}H_8)]_3$ and $PdCl_2$/$[NP(O_2C_{12}H_8)]_3$ on SiO_2. By varying the parameters: experimental setup, nature of metal precursor, the $MLn/N_3P_3(O_2C_{12}H_8)_3$ ratio, or the substrate, solid Pd and Ag nanoparticles or metal foams can be obtained and easily incorporated in another solid matrix for potential application in high throughput combinatorial applications, catalysis and water purification. Importantly, the method allows the growth of metallic materials in the complete absence of water or liquids.

Acknowledgments

Financial support by FONDECYT (projects 1085011, 1120179 and 1130416) is gratefully acknowledged. The authors thank Dr Calum Dickinson for assistance with HRTEM measurements. COD acknowledges support by Science Foundation Ireland under contract no. 07/SK/B1232a, the UCCC Strategic Research Fund and the Irish Research Council New Foundations Award 2012.

Appendix A. Supplementary data

Supplementary data related to this article can be found at http://dx.doi.org/10.1016/j.matchemphys.2013.08.034.

References

[1] A.S. Edelstein, R.C. Cammarata, Nanomaterials: Synthesis Properties and Applications, J.W. Arrowsmith Ltd, Bristol, 2000.
[2] K.J. Klabunde, Nanoscale Materials in Chemistry, Wiley, Interscience, New York, 2001.
[3] C.N. Rao, A. Muller, A.K. Cheetham (Eds.), The Chemistry of Nanomaterials, Synthesis, Properties and Applications, Wiley-VCH, Weinheim, 2004.
[4] J. Turkevich, P.C. Stevenson, J. Hillier, Discuss. Faraday Soc. 11 (1951) 55.
[5] M. Brust, M. Walter, D. Berthell, D. Schiffrin, R. Whyman, J. Chem. Soc. Chem. Commun. (1994) 801.
[6] For a discussion on solid-state preparation methods of nanoparticles see: C. Díaz, M.L. Valenzuela en, in: H.S. Nalwa (Ed.), "Metallic Nanostructures Using Oligo and Polyphosphazenes as Template or Stabilizer in Solid State" en Encyclopedia of Nanoscience and Nanotechnology, vol. 16, American Scientific Publishers, 2011, pp. 239–256.
[7] J. Turkevich, G. Kim, Science 169 (1970) 873.
[8] D.A. Alonso, C. Wajero, Chem. Soc. Rev. 39 (2010) 2891.
[9] J.G. de Vries, J. Chem. Soc. Dalton Trans. 421 (2006).
[10] T. Teranishi, M. Miyake, Chem. Mater. 10 (1998) 594.
[11] P. John Thomas, G.U. Kulkarni, C.N.R. Rao, J. Phys. Chem. 104 (2000) 8138.
[12] Y. Sun, L. Zhang, H. Zhou, Y. Zhu, E. Sutter, Y. Yi, M.H. Rafailovich, J.C. Socolov, Chem. Mater. 19 (2007) 2065.
[13] M.T. Reetz, W. Helbig, J. Am. Chem. Soc. 116 (1994) 7401.
[14] E. Ramirez, S. Jansat, K. Philippot, P. Lecante, M. Gomez, A.M. Masdeu-Bulto, B. Chaudret, J. Organomet. Chem. 689 (2004) 4601.
[15] N. Arul Dhas, A. Gedanken, J. Chem. Mater. 8 (1998) 445.
[16] G. Cardenas-Trivino, K.J. Klabunde, E.B. Dale, Langmuir 3 (1987) 986.
[17] Y. Yu, Y. Zhao, T. Huang, H. Liu, Pure Appl. Chem. 81 (2009) 2377.

[18] H. Chen, G. Wei, A. Ispas, S.G. Hickey, A. Eychmuller, J. Phys. Chem. C 114 (2010) 21976.
[19] Y. Xiong, B. Wiley, J. Chen, Z.Y. Li, Y. Ying, Y. Xia, Angew. Chem. Int. Ed. 44 (2005) 7913.
[20] J.M. Yuk, J. Park, P. Ercius, K. Kim, D.J. Hellebusch, M.F. Crommie, J.Y. Lee, A. Zettl, A.P. Alivisatos, Science 336 (2012) 61.
[21] M.R. Langille, J. Zhang, M.L. Personick, S. Li, C.A. Mirkin, Science 337 (2012) 954.
[22] T.K. Sau, A.L. Rogach, Complex Shaped Metal Nanoparticles – Bottom-up Syntheses and Applications, Wiley-VCH, Weinheim, Germany, 2012.
[23] J. Zhang, M.R. Langille, C.A. Mirkin, Nano Lett. 11 (2011) 2495.
[24] D. Jose, B.R. Jagirdar, J. Solid State Chem. 183 (2010) 2059.
[25] R. Diaz-Ayala, L. Arroyo, R. Raptis, C.R. Cabrera, Langmuir 20 (2004) 8329.
[26] J.E. Millstone, S.J. Hurst, G.S. Metraux, J.I. Cutler, C.A. Mirkin, Small 5 (2009) 646.
[27] Y. Sun, Y. Xia, Science 298 (2002) 2176.
[28] I. Pastoriza-Santos, R.A. Alvares-Puebla, L. Liz-Marzan, Eur. J. Inorg. Chem. (2010) 4228.
[29] B.L. Cushing, V.L. Kolesnichenko, Ch. O'Connor, Chem. Rev. 104 (2004) 3893.
[30] S. Navaladian, B. Viswanathan, T.K. Varadarajan, R.P. Viswanath, Nanotechnology 19 (2008) 045603.
[31] P. Dallas, A.B. Bourlinos, P. Komninou, M. Karakassides, D. Niarchos, Nanoscale Res. Lett. 4 (2009) 1358.
[32] M. Kariniemi, J. Niinisto, T. Hatanpaa, M. Kemell, T. Sajavaara, M. Ritala, M. Leskela, Chem. Mater. 23 (2011) 2901.
[33] G. Walkers, I.P. Parkin, J. Mater. Chem. 19 (2009) 574.
[34] G.B. Khomutov, V.V. Kislov, M.N. Antipirina, R.V. Gainutdinov, S.P. Gubin, A.Y. Obydenov, S.A. Pavlov, A.A. Rakhnyanskaya, A.N. Sergeev-Cherenkov, E.S. Soldatov, D.B. Suyatin, A.L. Toltikhina, A.S. Trifonov, T.V. Yurova, Microelectron. Eng. 69 (2003) 373.
[35] A. Tricoli, M. Righettoni, A. Teleki, Angew. Chem. Int. Ed. 49 (2010) 7632.
[36] S.A. Chambers, Adv. Mater. 21 (2009) 1.
[37] A.M. Hodge, J.R. Hayes, J.A. Caro, J. Biener, A.V. Hamza, Adv. Eng. Mater. 8 (2006) 853.
[38] B.C. Tappan, M.H. Huyuh, M.A. Hiskey, D.E. Chavez, E.P. Luther, I.T. Mang, S.F. Son, J. Am. Chem. Soc. 128 (2006) 6589.
[39] I. Banhart, Adv. Eng. Mater. 8 (2006) 781.
[40] H. Zhang, A.I. Cooper, J. Mater. Chem. 15 (2005) 2157.
[41] J. Biener, A. Wittstock, L.A. Zepeda-Ruiz, M.M. Biener, M.M. Zielasek, D. Kramer, R.N. Viswanath, J.K. Weissmuller, M. Baumer, A.V. Hamza, Nat. Mater. 1 (2009) 47.
[42] A. Cooper, Adv. Mater. 15 (2003) 1049.
[43] Y. Ding, J. Enlebacher, J. Am. Chem. Soc. 125 (2003) 772.
[44] F. Khan, S. Mann, J. Phys. Chem. C 113 (2009) 19871.
[45] J. Biener, A. Hodge, J. Hayes, C. Volkert, L. Zepeda, A. Hamza, F. Abrahm, Nano Lett. 6 (2006) 2379.
[46] C. Díaz, M.L. Valenzuela, L. Zuñiga, C. O'Dwyer, J. Inorg. Organomet. Polym. 19 (2009) 507.
[47] J. Jimenez, A. Laguna, M. Benouazzane, J.A. Sanz, C. Díaz, M.L. Valenzuela, P.G. Jones, Chem. Eur. J. 15 (2009) 13509.
[48] C. Diaz, M.L. Valenzuela, D. Bravo, V. Lavayen, C. O'Dwyer, Inorg. Chem. 47 (2008) 11561.
[49] C. Díaz, M.L. Valenzuela, Macromolecules 39 (2006) 103.
[50] C. Díaz, P. Castillo, M.L. Valenzuela, J. Cluster Sci. 16 (2005) 515.
[51] C. Díaz, M.L. Valenzuela, J. Inorg. Organomet. Polym. 16 (2006) 123.
[52] C. Díaz, M.L. Valenzuela, J. Inorg. Organomet. Polym. 16 (2006) 419.
[53] C. Díaz, M.L. Valenzuela, S. Ushak, V. Lavayen, C. O'Dwyer, J. Nanosci. Nanotechnol. 9 (2009) 1825.
[54] C. Diaz, J. Chil. Chem. Soc. 50 (2005) 417.
[55] C. Díaz, M.L. Valenzuela, A. Laguna, V. Lavayen, C.O. Dwyer, Langmuir 26 (2010) 10223.
[56] C. Díaz, V. Lavayen, C. O'Dwyer, J. Solid State Chem. 20 (2010) 1595.
[57] C. Diaz, M.L. Valenzuela, V. Lavayen, C. O'Dwyer, Inorg. Chem. 51 (2012) 6228.
[58] C. Diaz Valenzuela, M.L. Valenzuela, S. Caceres, C. O'Dwyer, J. Mater. Chem. A 1 (2013) 1566.
[59] C. Diaz, G.A. Carriedo, M.L. Valenzuela, L. Zuñiga, C. O'Dwyer, J. Inorg. Organomet. Polym. 22 (2012) 447.
[60] M. Capdevilla, W. Clegg, R.A. Coaxall, M. Gonzalez-Duarte, M. Hamidi, A. Ledos, G. Ujaque, Inorg. Chem. Commun. 1 (1998) 446.
[61] G.A. Carriedo, L. Fernández-Catuxo, F.J. García-Alonso, P. Gòmez-Elipe, Macromolecules 29 (1996) 5320.
[62] G. Reiter, Phys. Rev. Lett. 68 (1992) 75.
[63] R. Xie, A. Karim, J.F. Douglas, C.C. Han, R.A. Weiss, Phys. Rev. Lett. 8 (1998) 1251.
[64] A.M. Higgins, R.A.L. Jones, Nature 404 (2000) 476.
[65] H. Alhummiany, S. Jarvis, R.A.J. Woolley, A. Stannard, M. Blunt, P. Moriarty, J. Mater. Chem. 21 (2011) 16983.
[66] C. Diaz, M.L. Valenzuela, D. Bravo, V. Lavayen, C. O'Dwyer, J. Colloid Interface Sci. 362 (2011) 21.
[67] Benito Rodríguez-González, Farah Attouchi, M. Fernanda Cardinal, Viktor Myroshnychenko, Odile Stéphan, F. Javier García de Abajo, Luis M. Liz-Marzán, Mathieu Kociak, Langmuir 28 (2012) 9063.
[68] Chih-Ching Huang, Zusing Yang, Huan-Tsung Chang, Langmuir 20 (2004) 6089.